High Power Continuous Wave Nd:KGW Laser With Low Quantum Defect Diode Pumping

By

Rubel Chandra Talukder

A Thesis submitted to the Faculty of Graduate Studies of

The University of Manitoba

In partial fulfillment of the requirements of the degree of

MASTER OF SCIENCE

Department of Electrical and Computer Engineering

University of Manitoba

Winnipeg

Abstract

High power diode-pumped solid state (DPSS) lasers are a rapidly growing technology that is attractive for various applications in scientific and industrial fields. DPSS lasers are highly efficient, reliable and durable with superior beam quality when compared to flash-lamp pumped solid state lasers. Double-tungstate crystal of neodymium-doped potassium gadolinium tungstate (Nd:KGW) is one of the most effective active media used in DPSS lasers for generation of continuous wave radiation and ultrashort (i.e. picosecond, 10^{-12} s) pulses.

Unfortunately, the thermal conductivity of KGW host crystals is relatively low (~3 $Wm^{-1}K^{-1}$). This low thermal conductivity and large quantum defect while pumping with ~808 nm lead to significant thermo-optical distortions. One way to minimize thermo-optical distortions is to reduce the quantum defect. This can be done by pumping at longer wavelengths as compared to conventional 808 nm.

In this work we demonstrate what we believe is the first continuous wave Nd:KGW laser with hot band diode pumping at ~910 nm. This pumping wavelength reduced the quantum defect by >46% as compared to the conventional ~808 nm pumping and resulted in significantly lower thermal lensing. The laser produced 2.9 W of average output power at 1067 nm in a diffraction limited beam for an absorbed pump power of 8.3 W. The slope efficiency and optical-to-optical efficiency were found to be 43% and 35%, respectively. Significant reduction of quantum defect offered by this pumping wavelength and availability of suitable high power laser diodes opens an attractive way to further power and efficiency scaling of the Nd:KGW lasers.

Acknowledgements

First of all, I would like to thank my advisor, Dr. Arkady Major, for giving me the opportunity to engage in a very interesting research project. During my master's program, I have learned a lot from him, not only the academic and professional knowledge but also the positive attitude towards scientific research. I really appreciate his guidance and contribution in this research as well as his support in my daily life here in Canada.

I would also like to extend my gratitude to my M.Sc. committee members Dr. Cyrus Shafai and Dr. Can-Ming Hu for taking the time to review my thesis and participate in my defense.

I wish to express my gratitude to Government of Manitoba, Natural Sciences and Engineering Research Council (NSERC) and University of Manitoba for their financial support.

I really enjoyed the time spent working and discussing with my colleagues T. Waritanant, Md. Z. E. Halim, S. Manjooran and R. Akbari. A sincere thank you goes to them.

Keeping the best for the last, I would like thank my parents and specially my little brother Kutu.

Table of Contents

Abstract ..... **ii**

Acknowledgements ..... **iii**

Table of Contents ..... **iv**

List of Figures ..... **vi**

List of Tables ..... **viii**

Chapter 1: Introduction **9**

1.1 Motivation 9

1.2 Objectives 2

1.3 Contributions 2

1.4 Outline of the thesis 2

Chapter 2: Background information **4**

2.1 Thermal lensing 4

2.2 Low quantum defect pumping 7

2.3 Nd:KGW laser crystal 9

2.3.1 Crystal structure of Nd:KGW 9

2.3.2 Physical, thermal and optical properties of Nd:KGW 10

2.3.3 Spectroscopic properties of Nd:KGW 15

2.4 Previous results 19

Chapter 3: Experimental setup and results **21**

3.1 Pump laser diode 21

3.2 Laser cavity design 23

3.3 CW laser 26

3.3.1 CW results 29

3.4 Thermal lensing measurement 34

3.4.1 Thermal lensing results 34

Chapter 4: Conclusion and future work 39

References 40

List of Figures

Figure 2.1- Schematic diagram of quantum defect of a four level laser 5

Figure 2.2- Schematic diagram of thermal lens formation 6

Figure 2.3- a) Energy levels of Nd:YVO4 crystal, b) Output power vs. absorbed pump power [16]. 8

Figure 2.4- a) Orientation of optical indicatrix axes and crystallographic axes in a KGW crystal [24], b) Nd:KGW crystal used in our experiment (wrapped in indium foil). 10

Figure 2.5- Energy levels of Nd:KGW crystal [21]. 15

Figure 2.6- Polarized absorption spectra of Nd:KGW crystal at room temperature [25]. 16

Figure 2.7- Fluorescence spectra of Nd:KGW around 900 nm [29]. 17

Figure 2.8- Polarized emission spectra of Nd:KGW crystal at room temperature [25]. 18

Figure 3.1- Output power of pump diode vs. drive current 21

Figure 3.2- a) Laser diode wavelength vs. drive current, b) diode spectrum at 8A of current. 22

Figure 3.3- Lens equivalent laser cavity 23

Figure 3.4- Beam radius inside the laser cavity 24

Figure 3.5- Stability diagram against the focal length of the thermal lens 25

Figure 3.6- Beam radius variation at the output coupler with respect to focal length of the thermal lens. 26

Figure 3.7- a) Nd:KGW crystal dimension, b) Experimental setup for continuous wave operation. 27

Figure 3.8- a) Water cooling mount of the Nd:KGW laser crystal, b) a typical experimental laser setup. 28

Figure 3.9- a) Measured output power with linear fit, b) CW laser spectrum. 31

Figure 3.10- Percentage of absorbed pump power vs. incident pump power. 32

Figure 3.11- Measurement of beam radius variation. 33

Figure 3.12- Laser beam quality at 2.9 W of output power. Inset: transverse intensity profile of the laser beam. 33

Figure 3.13- Laser output beam quality M^2 at output power of 1.6 W and 2.7 W. 35

Figure 3.14- Output power and beam quality factor values vs. absorbed pump power. 36

Figure 3.15- Thermal lens focusing power with respect to absorbed pump power. 36

List of Tables

Table 2.1- Parameters of the unit cell of KGW 9

Table 2.2- Mechanical parameters of KGW crystal 11

Table 2.3- Principal refractive indices for pure and Nd-doped KGW at 1.06 μm..... 11

Table 2.4- Thermal expansion coefficients of pure and Nd-doped KGW 12

Table 2.5- Thermal conductivity of pure and Nd-doped KGW 12

Table 2.6- Thermo-optic coefficient dn/dT (10^{-6} K^{-1}) for pure and Nd-doped KGW crystals 14

Table 2.7- Polarized absorption cross sections at peak absorption wavelengths for Nd:KGW crystal 16

Table 2.8- Polarized stimulated-emission cross sections at peak fluorescence wavelengths for Nd:KGW crystal 18

Table 2.9- Comparison of spectroscopic properties of Nd:KGW with Nd:YVO4 and Nd:YAG 19

Table 3.1- Parameters used in the laser cavity design 23

Table 3.2- Comparison of CW results 29

Table 3.3- Comparison of thermal lens focusing power 37

Chapter 1: Introduction

1.1 Motivation

Lasers have been used in many diverse applications in medical, scientific and industrial fields since the first demonstration of laser in 1960. High intensity, high directionality and high degree of coherence are some of the unique properties of laser radiation. Moreover, solid state lasers and especially diode-pumped solid state lasers (DPSS) lasers are highly efficient, reliable and durable with excellent beam quality.

One of the most effective laser gain media is neodymium-doped potassium gadolinium tungstate crystal (Nd:KGW) for solid state laser engineering in the near-infrared region. Nd:KGW has some exceptional properties compared with other widely used Nd^{3+} doped laser crystals operating around 1 μm such as Nd:YAG and Nd:YVO. High doping concentration of Nd^{3+} ion and high slope efficiency can be achieved with it [1]. This crystal is well known for its high emission cross section (higher than that of Nd:YAG) and thus efficient continuous wave (CW) [2], Q-switched [3] and mode-locked operation [4, 5]. In addition, birefringence of the host results in strongly polarized emission which is advantageous for further frequency conversion [6, 7, 8]. Owing to the high third-order nonlinearity of the host [9, 10], Nd:KGW crystals and lasers are widely used to generate multiple wavelengths via stimulated Raman scattering [6, 7]. Continuous wave Raman lasing based on Nd:KGW crystal was also reported [11].

Unfortunately, the relatively low thermal conductivity (about half that of Nd:YVO) of KGW host crystals and large quantum defect (with ~808 nm pumping) lead to significant thermo-optical distortions. As a result of thermal effects, the power scaling to multi-watt level is hindered [12]. Therefore, reduction of thermal lensing is the key strategy to achieve power scaling. This can be done by pumping at longer wavelengths (as compared to traditional 808 nm) to reduce the quantum defect. Although pumping at around 880 nm was reported [13, 14, 15], this is not the longest possible pump wavelength for Nd-ion based gain media. Recently, efficient diode pumping (at 914 nm) of a Nd:YVO laser from the highest thermally populated sublevel (i.e. hot band) of the ground state manifold was realized, thus enabling slope efficiency to reach up to 81% in the CW [16]

regime and up to 77% in the mode-locked regime [17]. It was also shown that such a long wavelength pumping reduced thermal lensing by a factor of two [18] in comparison with 808 nm pump wavelength.

Therefore, we use similar approach of hot band diode pumping to demonstrate a multi-Watt CW Nd:KGW laser.

1.2 Objectives

The objective of this work is to demonstrate a multi-watt continuous wave Nd:KGW laser with hot band diode pumping at around 910 nm. Traditional pumping of Nd:KGW at ~808 nm leads to significant thermal effects. This is the main obstacle to multi-watt power scaling of Nd:KGW lasers. Hot band diode pumping at ~910 nm can minimize the thermal effects and as a result will enable high power operation of the Nd:KGW crystal. Therefore, this work has the potential to open a promising route to power scaling of Nd:KGW lasers.

1.3 Contributions

The following contribution has been made in this work:

A multi-Watt continuous wave operation of a Nd:KGW laser at 1067 nm with hot band diode pumping was demonstrated. To the best of our knowledge, this is the first time that this approach was used with Nd:KGW laser crystal. The results of this work were presented at the Photonics North 2016 conference [19] and at the Conference on Lasers and Electro-Optics (CLEO) [20]. They were also accepted for publication in peer-reviewed Optics Letters journal [21]].

1.4 Outline of the thesis

Background information used in this thesis will be explained in chapter 2. Chapter 2 will start with the description of thermal lensing. The idea of thermal lensing and what happens because of it will be discussed in this chapter. Next, low quantum defect pumping approach will be explained. In addition to that, the properties of Nd:KGW laser crystal will be introduced. Finally, the results of CW Nd:KGW laser with 808 and 880 nm pumping will be discussed.

Chapter 3 will present the experimental setup and results of our experiment. First, a description of the pump laser diode will be given. Then, the design of our laser cavity will be discussed. Moreover, CW results and beam quality measurements will be presented and explained. At last, thermal lensing results will be discussed at the end of this chapter.

Chapter 4 of the thesis presents the conclusion and possible future work.

Chapter 2: Background information

2.1 Thermal lensing

Thermal lensing occurs due to the generation of heat in the laser gain medium. Heat generation in the process of optical pumping happens due to several reasons:

- The energy difference between the pump band and the upper laser level is converted into heat inside the laser crystal as shown in figure 2.1. Likewise, the energy difference between the lower laser level and the ground state is also lost as heat. Therefore, the energy difference between the pump photon and the laser photon is the major source of heating in solid state lasers and is termed as quantum defect. This can be written as

$$q = E_P - E_L = \frac{hc}{\lambda_{Pump}} - \frac{hc}{\lambda_{laser}} \quad (2.1)$$

Here, q = quantum defect;

E_P = energy of the pump photon;

E_L = energy of the laser photon;

λ_{Laser} = wavelength of laser radiation;

λ_{Pump} = wavelength of pump radiation;

c = speed of light;

Typical pumping of Nd:KGW crystal with ~808 nm ensures that 24% of the pump power will be converted into heat as the lasing wavelength is 1067 nm. Pumping with a wavelength longer than 808 nm will reduce the generated heat inside the crystal if the crystal still lases at 1067 nm.

A pictorial view of the quantum defect is shown below:

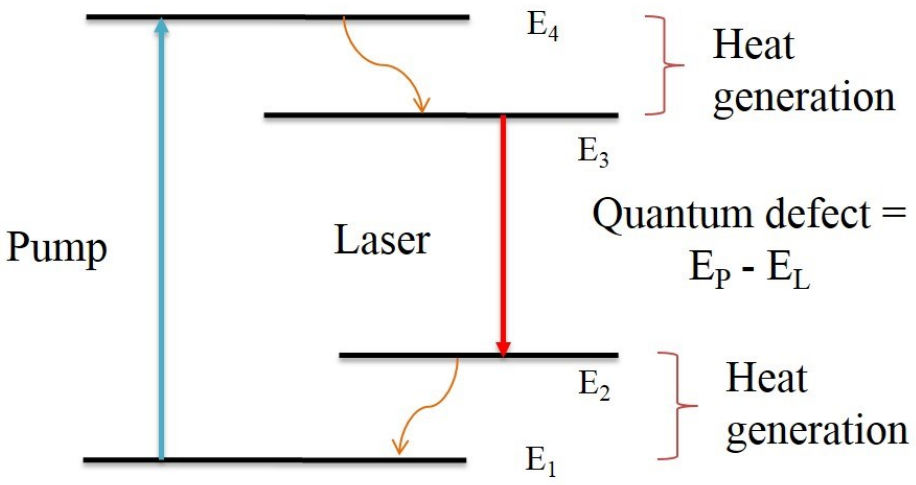

Figure 2.1- Schematic diagram of quantum defect of a four level laser

- Moreover, nonradiative relaxation is also a source of heat generation within the laser crystal. Nonradiative relaxation from the upper laser level E_3 to the ground state E_1 (due to concentration quenching) and nonradiative relaxation from the pump band E_4 to the ground state E_1 will generate heat in the active medium.

The generated heat results in a temperature gradient inside the laser crystal. The temperature gradient mainly induces two effects in the crystal: thermo-optic effect and thermo-mechanical effect. Refractive index changes due to temperature gradient inside the crystal and this phenomenon is known as the thermo-optic effect. Also, the thermo-mechanical effect generates mechanical stress inside the crystal through thermal expansion. The induced mechanical stress causes further change in refractive index which is called the photoelastic effect. Moreover, the mechanical stress produces the bulging of end faces of the crystal and in extreme cases could lead to crystal fracture. This thermally induced refractive index change and bulging deformation of end faces of the crystal cause a lensing effect which is known as thermal lensing [22]. A schematic diagram of thermal lens formation in shown in figure 2.2:

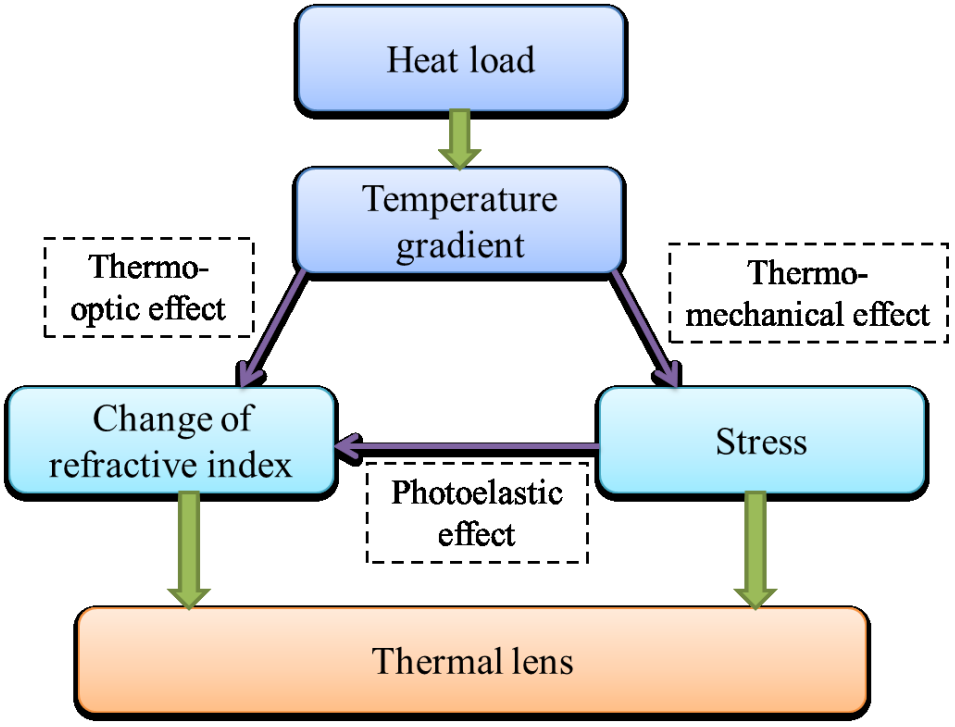

Figure 2.2- Schematic diagram of thermal lens formation

Basically, the three effects that result in thermal lensing are:

- Change of refractive index due to the temperature gradient which is described as thermo-optic effect.
- Induced mechanical stress due to the temperature gradient which is known as thermo-mechanical effect.
- Further change in refractive index due to the mechanical stress which is called the photoelastic effect [22].

Thermal lens can distort the laser beam size and wavefront when the beam passes through the crystal. A positive thermal lens will focus the laser beam while a negative thermal lens will defocus the beam. Also, spatial mode matching between the laser beam and pump beam inside the gain medium is important for lasing efficiency. Mode size variation induced by thermal lensing can

break mode matching between the laser and the pump beam. This mismatch will lead to low output power and low lasing efficiency.

Wavefront distortion adversely affects the output beam quality. Beam quality corresponds to the imperfection of a laser beam in comparison to the ideal fundamental beam (TEM_{00}).

The operating point of the laser cavity within the stability diagram becomes a function of input power due to thermal lensing. In extreme cases, the laser cavity can become unstable.

Above all, thermal lensing could lead to stress fracture and put a limit to average power obtainable from a laser medium [22]. As a result of the low thermal conductivity (about 3 $Wm^{-1}K^{-1}$) of Nd:KGW in combination with thermal lensing effects, high average power operation is hindered. We cannot modify thermal conductivity of a material; but we can lower the thermal effects by longer wavelength pumping as compared to conventional 808 nm pumping. Therefore, reduction of thermal effects is the main strategy to achieve power scaling.

2.2 Low quantum defect pumping

Low quantum defect pumping was studied with Nd:YVO_4 crystal [16]. The energy levels of this crystal are shown in figure 2.3(a). Usually Nd:YVO_4 is pumped with ~808 nm. Reduction of quantum defect requires pumping with longer wavelength. According to the figure 2.3(a), pumping was done from the thermally populated highest sublevel of the ground state manifold of the crystal in order to obtain low quantum defect as compared to the conventional 808 nm pumping. This pumping from the thermally populated sublevel is called the hot band pumping and it corresponds to 914 nm wavelength for the Nd:YVO_4 crystal. Hot band diode pumping enables us to reduce quantum defect and hence the thermal load inside the crystal.

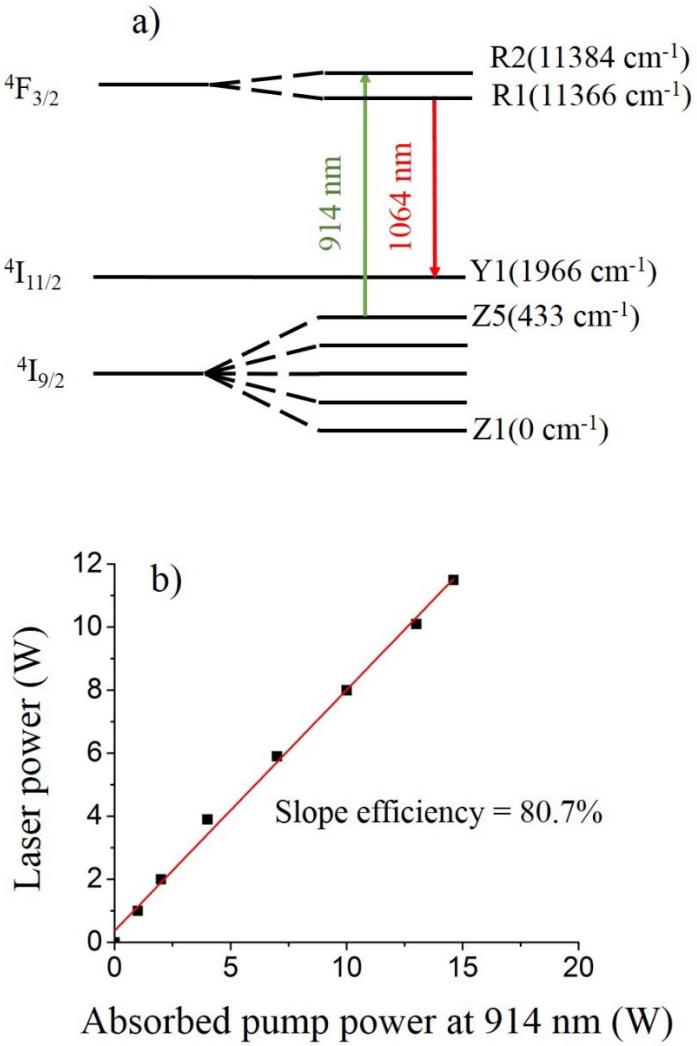

Figure 2.3- a) Energy levels of Nd:YVO4 crystal, b) Output power vs. absorbed pump power [16].

This pumping scheme provided some excellent results. The obtained output power was 11.5 W at 1064 nm for an absorbed pump power of 14.6 W as shown in figure 2.3(b). The slope efficiency was 80.7% which is very close to the theoretical maximum (85.9%). Also, optical to optical efficiency was 78.7% which was the highest optical efficiency ever reported for Nd:YVO_4 laser at this power level [16]. This high efficiency is a result of excellent overlap between the pump beam and the laser beam in the Nd:YVO_4 crystal.

The thermal lensing effects were very weak. The thermal lens focusing power was 0.6 diopter at maximum pump power which is one order of magnitude lower than the thermal lens measured around 800 mW of absorbed power at 808 nm. In addition, nearly a Gaussian ($M^2 = 1$) beam profile

was achieved in this experiment. Beam quality factor was 1.1 in the horizontal direction and 1.2 in the vertical direction [16].

Now, a similar approach can be also used to pump a Nd:KGW crystal in order to reduce the quantum defect. The hot band pumping was not studied with Nd:KGW crystal before. The hot band corresponds to the 910 nm wavelength for the Nd:KGW crystal as shown in figure 2.5. This 910 nm pumping ensures the lowest quantum defect as this wavelength corresponds to the highest sublevel of the ground state manifold for the Nd:KGW crystal. Therefore, lower thermal effects within the crystal can be obtained with hot band pumping as compared to the traditional 808 nm pumping.

2.3 Nd:KGW laser crystal

2.3.1 Crystal structure of Nd:KGW

The crystal structure of $KGd(WO_4)_2$ is monoclinic and it corresponds to the space group C^6_{2h}-C2/c which is defined as the symmetry group of a configuration in space, usually in three dimensions. Space groups are also called the crystallographic groups, and represent a description of the symmetry of the crystal [23]. The unit cell parameters of the KGW crystal are mentioned in table 2.1.

Table 2.1- Parameters of the unit cell of KGW

Reference	Unit cell parameters			
	a (Å)	b (Å)	c (Å)	β (deg)
Mochalov et al. [24]	8.098	10.417	7.583	94.43
Chen et al. [25]	10.652	10.374	7.582	130.8

The mutual orientation of the crystallographic axes (a, b, c) and the axes of the optical indicatrix (N_m, N_p, N_g) of the KGW crystal is shown in figure 2.4(a). From the figure, it is obvious that [010] is parallel to N_p. Besides, N_m and N_g axes make 24 and 20 degree angles with [100] and [001] axes, respectively [24]. Figure 2.4(b) also shows the laser crystal that was used in our experiment.

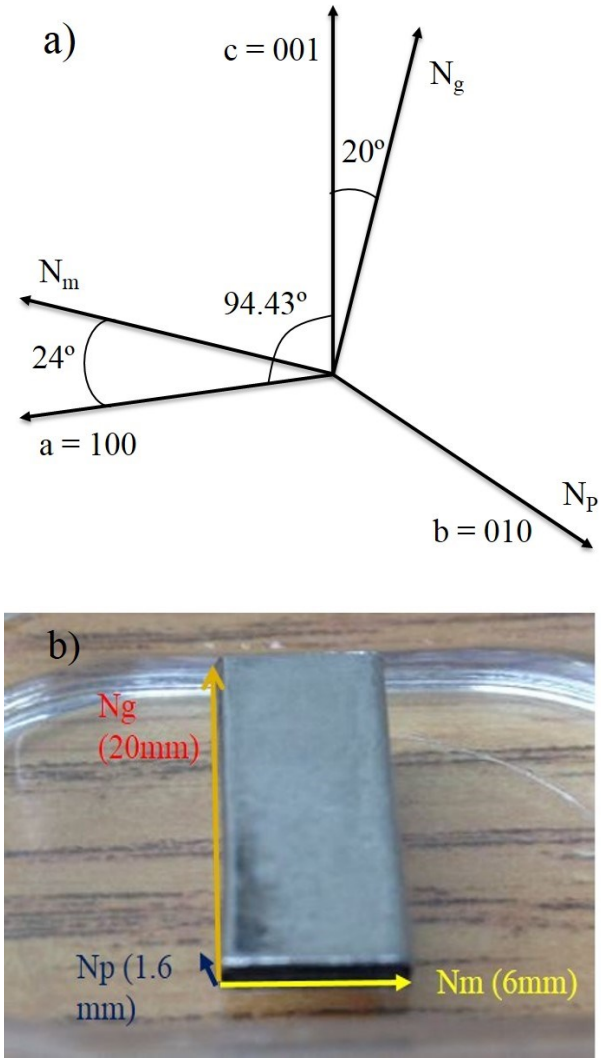

Figure 2.4- a) Orientation of optical indicatrix axes and crystallographic axes in a KGW crystal [24], b) Nd:KGW crystal used in our experiment (wrapped in indium foil).

2.3.2 Physical, thermal and optical properties of Nd:KGW

KGW crystal is highly anisotropic with three principal optical axes direction denoted as N_m, N_p and N_g. The crystal is anisotropic in its mechanical properties because of the monoclinic structure. Characterization of its physical, thermal and optical properties has attracted a lot of attention because it can be used as a host for a range of dopants. For example, doping with Yb-ions produces broadband radiation around 1030 nm that can be used for generation of powerful ultrashort pulses [26, 27, 28, 29] . Table 2.2 gives the approximate values of microhardness, ultimate strength, and Young's modulus in three principal directions of the crystal [24].

Table 2.2- Mechanical parameters of KGW crystal

Property	Value along [100]	Value along [010]	Value along [001]
Knoop microhardness (kg/mm^2)	370	390	460
Ultimate strength (kg/mm^2)	14	10.2	6.4
Young's modulus (GPa)	115.8	152.5	92.4

Table 2.3 shows the measured anisotropic values of the principal refractive indices of pure KGW and Nd-doped KGW published in various papers. It is obvious that for both measurements $n_p<n_m<n_g$.

Table 2.3- Principal refractive indices for pure and Nd-doped KGW at 1.06 μm

Reference	Doping	n_m	n_g	n_p
Mochalov et al. [24]	−	1.986	2.033	1.937
Graf et al. [2]	2.2%	2.014	2.049	1.978

Thermal conductivity, thermal expansion coefficients and thermo-optic coefficient (dn/dT) are the three major thermal properties of a laser material which play a very important role in thermal lens formation and therefore power scaling of solid state lasers.

The thermal expansion coefficient is defined as the change in the length of the laser crystal per unit temperature. Anisotropy of the Nd:KGW crystal ensures that the value of thermal expansion coefficient is different in different directions. Thermal expansion coefficients for pure and Nd-doped KGW crystal are listed in Table 2.4. The largest expansion occurs along [001] axis, while the lowest expansion occurs along [010] axis. The lower value of thermal expansion coefficient is better for high power solid state laser operation.

Table 2.4- Thermal expansion coefficients of pure and Nd-doped KGW

Reference	Doping	Value along [100]	Value along [010]	Value along [001]
Mochalov et al. [24]	−	4	1.6	8.5
Moncorge et al. [30]	3%	4	3.6	8.5
Graf et al. [2]	2.2%	4	3.6	8.5

Thermal conductivity refers to the ability of a material to transfer heat. Heat transfer is higher in materials with higher thermal conductivity and lower for lower thermal conductivity materials. Hence, high thermal conductivity is preferred for high power operation. Thermal conductivity of pure KGW and doped-KGW is presented in Table 2.5. It is seen from the table that KGW crystals have a moderate thermal conductivity of around 3 $Wm^{-1}K^{-1}$.

Table 2.5- Thermal conductivity of pure and Nd-doped KGW

Reference	Doping	Value along [100]	Value along [010]	Value along [001]
Mochalov et al. [24]	−	2.6	3.8	3.4
Esmeria et al. [31]	3-10%	2.8	2.2	3.5
Graf et al. [2]	2.2%	2.6	3.8	3.4

The thermo-optic coefficient (dn/dT) determines the temperature dependence of the refractive index in the laser material. It is the change in refractive index due to a change in temperature. Reported values of thermo-optic coefficients of pure and Nd-doped KGW are listed in table 2.6 at various wavelengths. According to Mochalov et al, the thermo-optic coefficients can be both positive and negative at 1060 nm. It is important to mention that dn/dT not only varies with operating wavelength but also depends on the observation direction. But, according to Loiko et al, the values of thermo-optic coefficients measured by a beam deflection method are negative in three directions. This implies that the principal refractive indices decrease with an increase in

temperature. As can be seen, there is still uncertainty in the sign of the thermo-optic coefficients which is most likely a result of experimental measurement errors.

Table 2.6- Thermo-optic coefficient dn/dT (10^{-6} K^{-1}) for pure and Nd-doped KGW crystals

Reference	Wavelength (nm)	Doping	Observation direction vector k	dn/dT ($E \| N_m$)	dn/dT ($E \| N_g$)	dn/dT ($E \| N_p$)
Mochalov et al. [24]	1060	–	N_m	–	-0.3	-1.9
			N_g	4.3	–	1.7
			N_p	-0.8	-5.5	–
Loiko et al. [12]	1064	–	N_m	–	-18.12	-16.11
			N_g	-12.93	–	-15.75
			N_p	-12.02	-17.20	–
		3 at %	N_m	–	-19.67	-16.46
			N_g	-11.99	–	-15.42
			N_p	-11.64	-19.31	–
	532	–	N_m	–	-16.52	-14.65
			N_g	-10.07	–	-14.02
			N_p	-9.44	-15.53	–
		3 at %	N_m	–	–	–
			N_g	-10.01	–	-14.25
			N_p	–	-14.98	–
Loiko et al. [12]	632.8	–	N_m	–	-16.48	-14.35
			N_g	-9.98	–	-14.14
			N_p	-9.39	-15.01	–
		3 at %	N_m	–	-16.07	-15.02
			N_g	-10.43	–	-14.56
			N_p	-9.84	-15.89	–

2.3.3 Spectroscopic properties of Nd:KGW

The energy levels of Nd:KGW are shown in figure 2.5 and were reported in [21]. Conventional pumping scheme involves pumping with radiation around 808 nm. Although pumping at around 880 nm was reported [13, 14, 15], this is not the longest possible pump wavelength for this crystal. We can also pump from the thermally populated highest sublevel of the ground state manifold (i.e. hot band) of Nd:KGW crystal. This sublevel corresponds to a wavelength around 910 nm and ensures the lowest possible quantum defect for this crystal. Therefore, hot band pumping is useful to reduce the quantum defect and can lead to a high power operation of the Nd:KGW crystal based laser.

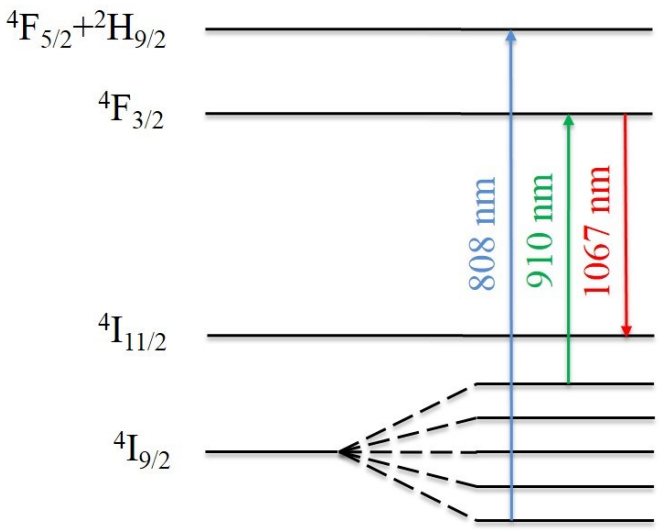

Figure 2.5- Energy levels of Nd:KGW crystal [21].

The polarized absorption spectra at room temperature of Nd:KGW are shown in figure 2.6 [25]. The polarization dependence of the absorption spectra arises from the anisotropic properties of the crystal. It is obvious from the figure 2.6 that the peak absorptions of the $^4I_{9/2}$ - $^4F_{5/2}+^2H_{9/2}$ transition were all located around 808 nm for all polarizations. The commercial laser diodes are available which emit around 808 nm. Also, the absorption cross section varies in different directions. The absorption cross section for E||Nm (26.75×10^{-20} cm^2) (where E is the electric field vector) is larger than those for E||Np (7.81×10^{-20} cm^2) and E||Ng (3.43×10^{-20} cm^2) directions as mentioned in table 2.7. The crystal with larger absorption cross section at a certain pump

wavelength means that it has higher absorption coefficient at a certain dopant concentration compared to a lower absorption cross section [25].

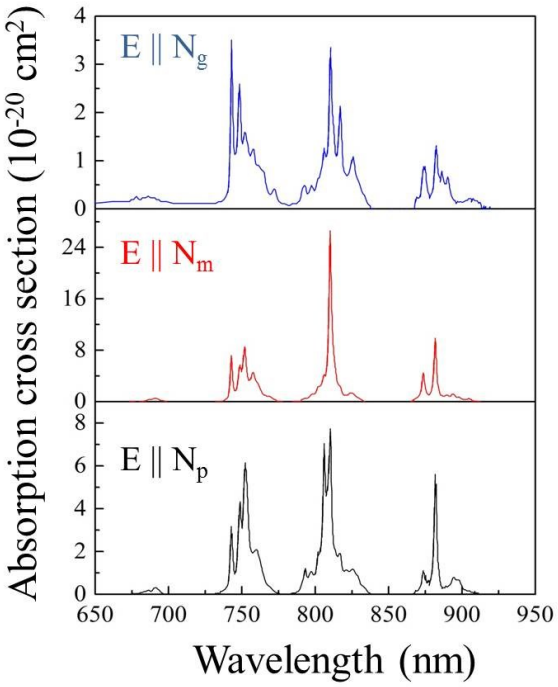

Figure 2.6- Polarized absorption spectra of Nd:KGW crystal at room temperature [25].

Table 2.7- Polarized absorption cross sections at peak absorption wavelengths for Nd:KGW crystal

$E \parallel N_g$		$E \parallel N_m$		$E \parallel N_p$	
λ_{abs} (nm)	$\sigma_{abs}(10^{-20}$ cm$^2)$	λ_{abs} (nm)	$\sigma_{abs}(10^{-20}$ cm$^2)$	λ_{abs} (nm)	$\sigma_{abs}(10^{-20}$ cm$^2)$
743	3.52	752	8.68	752	6.18
810	3.43	810	26.75	810	7.81
882	1.37	882	9.95	882	5.63

In this work we used pumping wavelength around 910 nm. This wavelength corresponds to an electron excitation from the thermally populated highest sublevel of the ground state manifold $^4I_{9/2}$ to the upper laser level $^4F_{3/2}$ as shown in figure 2.5. Since this sublevel can also be used as a quasi-

three-level laser transition, its potential for pumping can be evaluated from the fluorescence data if the absorption data are unavailable. This was the case for Nd:KGW and our motivation for using the 910 nm pumping wavelength came from the fluorescence spectra which are shown in figure 2.7 [30]. It is obvious from figure 2.7 that the Nd:KGW crystal fluoresces around 910 nm although it is not the strongest. Therefore, we can conclude that 910 nm can be used to pump this crystal as the absorption and fluorescence peaks coincide.

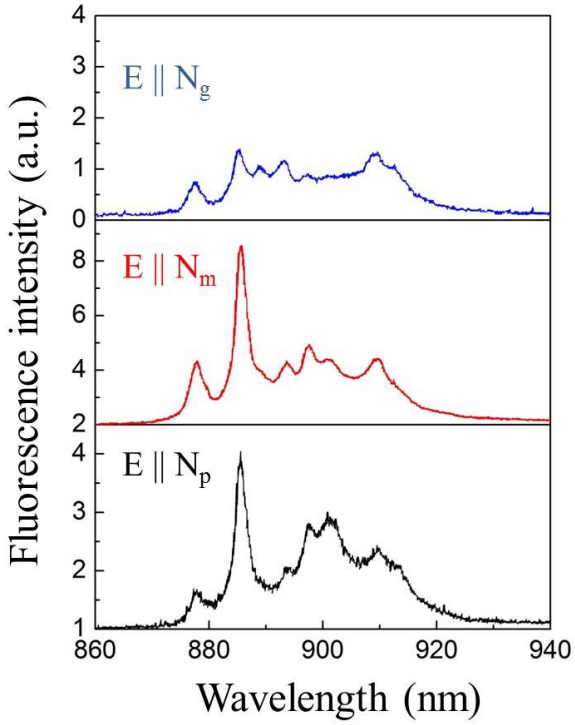

Figure 2.7- Fluorescence spectra of Nd:KGW around 900 nm [29].

The emission spectra of Nd:KGW crystal in different polarizations at room temperature are shown in figure 2.8 and mentioned in table 2.8 [25]. The strongest laser emissions are all located around 1067 nm for all three polarizations. The largest stimulated-emission cross section at 1067 nm is about 32.3×10^{-20} cm^2 for the E||Nm polarization. The laser output at 1067 nm is polarized which is good for applications like non-linear optical frequency conversion such as stimulated Raman scattering or second harmonic generation [6, 8, 10]. At the same time a polarization with lower emission cross section can be also used for enhanced energy storage which is beneficial for generation of powerful Q-switched pulses from lasers [32].

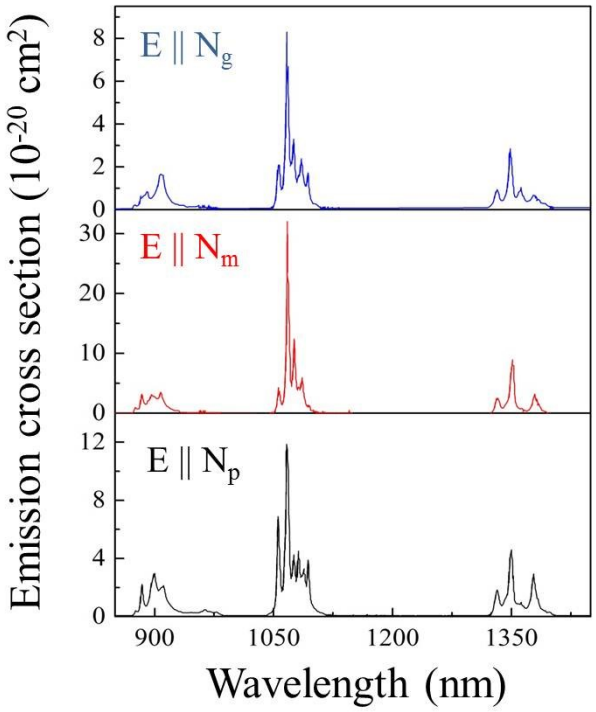

Figure 2.8- Polarized emission spectra of Nd:KGW crystal at room temperature [25].

Table 2.8- Polarized stimulated-emission cross sections at peak fluorescence wavelengths for Nd:KGW crystal

$E \parallel N_g$		$E \parallel N_m$		$E \parallel N_p$	
λ_{em} (nm)	$\sigma_{em}(10^{-20}$ cm$^2)$	λ_{em} (nm)	$\sigma_{em}(10^{-20}$ cm$^2)$	λ_{em} (nm)	$\sigma_{em}(10^{-20}$ cm$^2)$
908	1.67	907	3.70	899	3.01
1067	8.30	1067	32.26	1067	11.93
1349	2.84	1351	9.33	1350	4.62

Comparison of the main spectroscopic properties of the Nd:KGW crystal with the crystals of Nd:YVO_4 and Nd:YAG is shown in table 2.9 [25, 33]. Nd:KGW has some excellent properties when compared to other crystals. It has a broader gain bandwidth of 2.73 nm which is essential for

ultrashort pulse generation. Moderate emission cross section is still high enough to ensure low threshold power operation. On the other hand, the thermal conductivity of Nd:KGW crystal is lower than of the other laser crystals. The lower thermal conductivity acts as an obstacle for high power continuous wave operation. Therefore, low quantum defect pumping can be utilized to overcome the limitation imposed by the low thermal conductivity.

Table 2.9- Comparison of spectroscopic properties of Nd:KGW with Nd:YVO4 and Nd:YAG

Spectroscopic properties	Nd:KGW	$Nd:YVO_4$	Nd:YAG
Laser wavelength [nm]	1067	1064	1064
Emission cross section [10^{-20} cm^2]	32.3	250	28
Gain bandwidth [nm]	2.73	0.96	0.6
Fluorescence lifetime [μs]	110 at 3% doping	90 at 1% doping	230 at 1% doping
Thermal conductivity [$Wm^{-1}K^{-1}$]	~ 3	~ 5	14

2.4 Previous results

Continuous wave Nd:KGW lasers pumped by 808 nm [2, 30, 34, 35] and 880 nm [14, 35] diodes were reported previously. Moreover, thermal lensing was studied under both 808 nm and 880 nm diode pumping [13]. Pumping with longer than 880 nm wavelength to reduce quantum defect even further was not demonstrated. But, the same concept was used to pump a similar laser crystal $Nd:YVO_4$ [16]. $Nd:YVO_4$ was pumped by a 914 nm laser diode which corresponds to the highest sublevel of the ground state manifold which is also known as hot band.

The highest output power achieved with 808 nm pumping in CW regime was 3.25 W and reported by Abdolvand et al. [36] in 2010. The slope efficiency in that work was 74% and optical to optical efficiency was 66% at 1067 nm laser emission. The highest slope efficiency achieved with 808 nm pumping in CW regime was 75% and demonstrated by Boulon et al. in 2003 [37].

Also Graf et al. published their results of CW Nd:KGW crystal with 808 nm pumping [2]. The output power was 1.5 W with slope and optical-to-optical efficiency of 46% and 48.4%, respectively.

Nd:KGW crystal was also pumped with 880 nm by Bui et al. [15]. The 880 nm pumping reduced quantum defect when compared to 808 nm pumping done by Abdolvand et al. and Boulon et al. A simple two mirror cavity was designed to get 9.4 W of average output power in CW operation. The laser emission was around 1067 nm. The slope and optical efficiency were found to be 66.4% and 63.9%, respectively.

The crystal can be also pumped with a longer wavelength than 880 nm. Hot band diode pumping with 910 nm will reduce quantum defect even further than 880 nm and, therefore, can lead to higher output power and slope efficiency. Moreover, the thermal effects will also be weaker for a hot band pumping.

Chapter 3: Experimental setup and results

3.1 Pump laser diode

A 16 W high power fiber-coupled laser diode operating around 910 nm (~5 nm linewidth) was used as a pump source. The fiber had a core diameter of 110 μm and a numerical aperture of 0.12. The laser diode module emitted unpolarized light. This unpolarized output was first collimated with an f = 40 mm collimator lens and subsequently focused onto the laser crystal by an f = 200 mm focusing lens, producing a pump spot diameter of ~550 μm. The output power from the pump diode was measured at different drive currents and the results are shown in figure 3.1. The maximum output power obtained from the pump diode was about 16 W at 10 A drive current and 32 W of input electrical power. The electrical-to-optical efficiency of the pump diode was 50%.

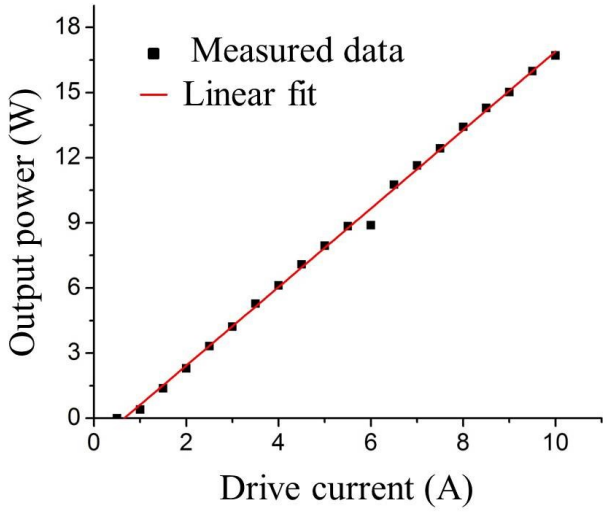

Figure 3.1- Output power of pump diode vs. drive current

The spectrum of the pump laser diode was analyzed using an optical spectrum analyzer. The wavelength of the laser diode changed with the drive current as shown in figure 3.2(a). The wavelength shifted towards longer wavelengths as we increased the drive current. Increased drive current also increased the temperature of the laser diode. For this reason the pump diode needed to be cooled at a certain temperature for a fixed wavelength operation. The spectrum of the pump

diode was measured for different drive currents. A typical spectrum of the diode is shown in figure 3.2(b) when driven with a current of 8A.

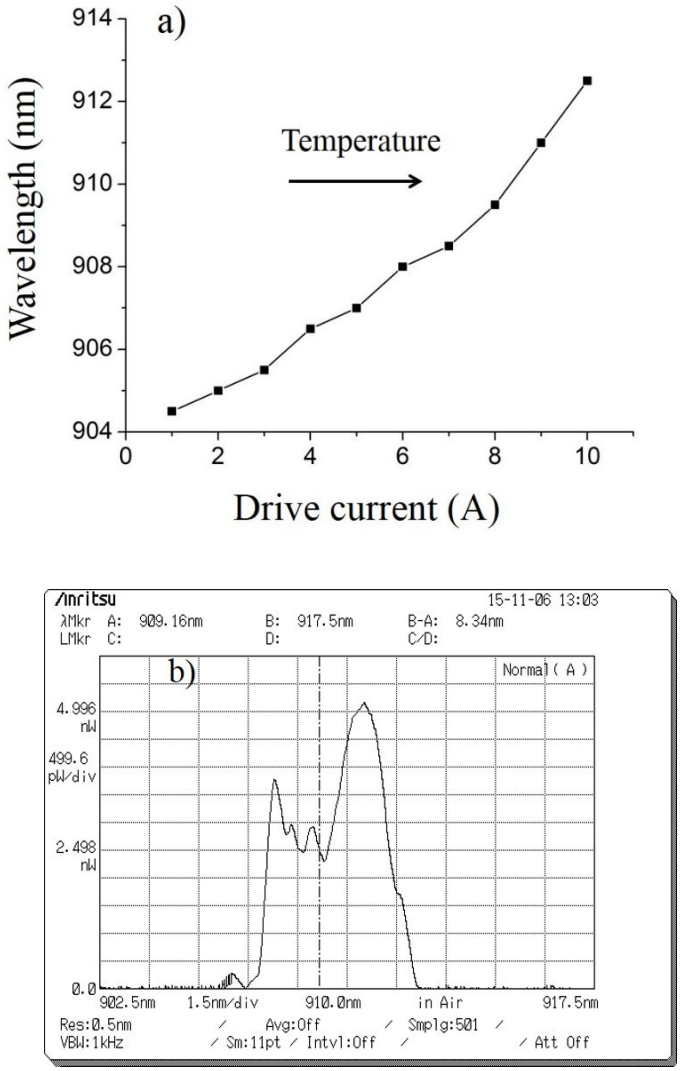

Figure 3.2- a) Laser diode wavelength vs. drive current, b) diode spectrum at 8A of current.

3.2 Laser cavity design

A z-cavity was designed and simulated using commercial reZonator software [38] before building of the laser system in the laboratory. The cavity was designed using an ABCD matrix analysis technique while the effect of thermal lensing was taken into account. The ABCD matrix related to an optical element is a 2-by-2 matrix which explains the element's effect on a laser beam [22]. A good overlap between the pump and the cavity modes was considered during the design to achieve an efficient laser system.

Table 3.1- Parameters used in the laser cavity design

Cavity Parameters								
	L1	L2	L3	L4	Crystal	R2	R4	L_T
Length (mm)	315	455	481	462	20	400	500	1733
n	1	1	1	1	2.17	–	–	–

The parameters used to design a laser cavity with desirable beam waists are shown in Table 3.1. These parameters are based on the lens equivalent cavity shown in figure 3.3, where curved mirrors are replaced by the equivalent lens elements for the purpose of ABCD matrix analysis. Here, R2 and R4 correspond to the radius of curvature of mirrors M2 and M4 respectively. The front mirror M1 is 100% reflective and the end mirror (which is the output coupler) is partially reflective. The output coupler (OC) usually reflects most of the light back inside the cavity and transmits some portion of the light as the laser output. The laser cavity was designed in a way that ensures the mode matching between the pump beam and the laser beam. In order to do so, we needed to find the beam radius at the crystal after one round trip. For a stable laser cavity, the laser beam should repeat itself after one round trip.

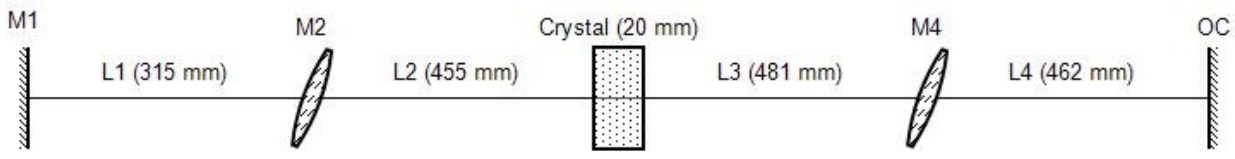

Figure 3.3- Lens equivalent laser cavity

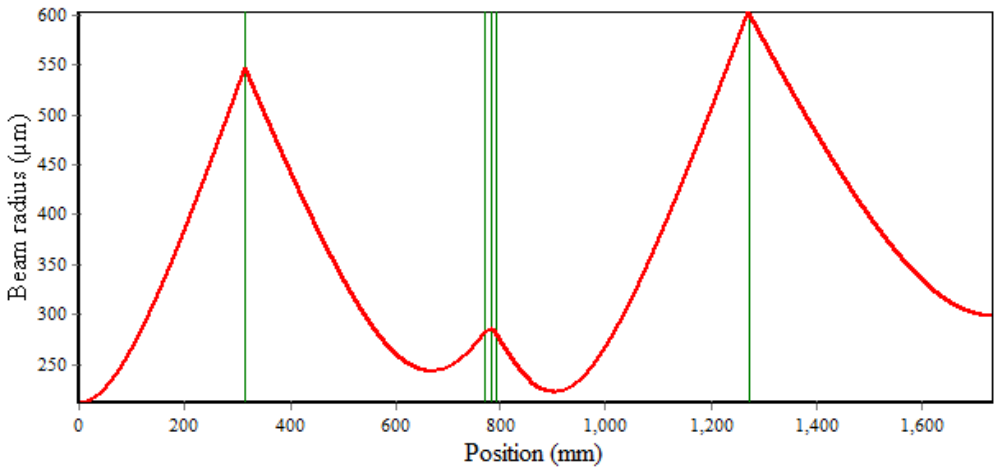

Figure 3.4- Beam radius inside the laser cavity

The simulated beam radius variation in the laser cavity is shown in figure 3.4. Therefore, according to the figure 3.4, the beam radius at the crystal is approximately 275 µm after one round trip. The pump beam should be very close to 275 µm at the crystal as well to ensure a good mode matching between the pump beam and the laser beam.

Not only the mode matching between the pump and the laser beam, but also thermal lensing needed to be taken into account for stable and efficient laser operation. Thermal lensing can be modeled as a thin lens inside the crystal. The strength of the thermal lens focusing power has a significant effect on stability of the cavity. The stability of the cavity determines whether the laser beam will be confined within the cavity or not. In a stable cavity, the laser beam will be confined within the cavity. By contrast an unstable cavity does not resonate the laser beam in the cavity. The stability of the laser cavity was simulated against the focal length of the thermal lens and is shown in figure 3.5.

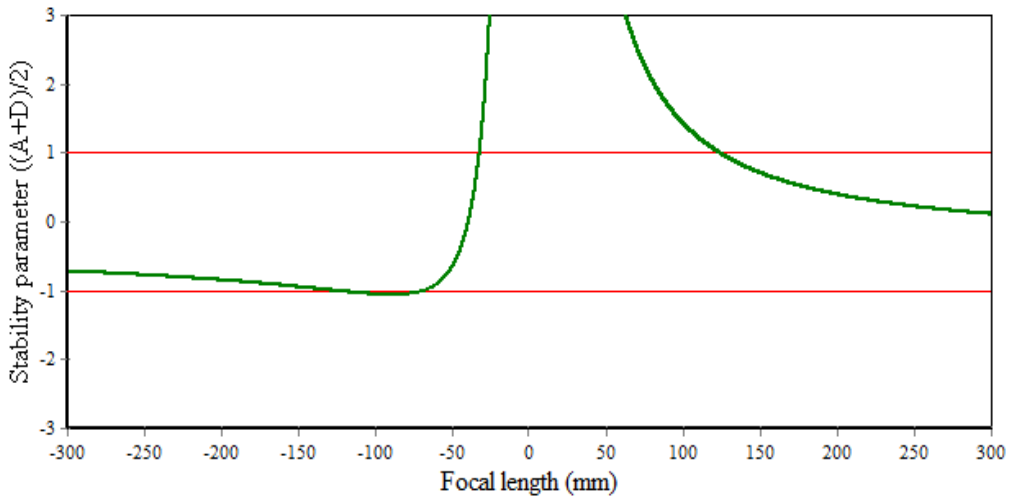

Figure 3.5- Stability diagram against the focal length of the thermal lens

The stable cavity must have the stability parameter in-between -1 and +1. The stability parameter is defined as (A+D)/2 [22]. It is obvious from the diagram that a focal length of -30 mm to 125 mm corresponds to an unstable laser cavity. Any other focal length of the thermal lens will lead to a stable cavity.

The beam radius variation at the output coupler with respect to focal length of the induced thermal lens is shown in Figure 3.6. According to the figure, both strong positive and negative thermal lensing results in the increase of output mode radius at the output coupler which can lead to an unstable laser cavity.

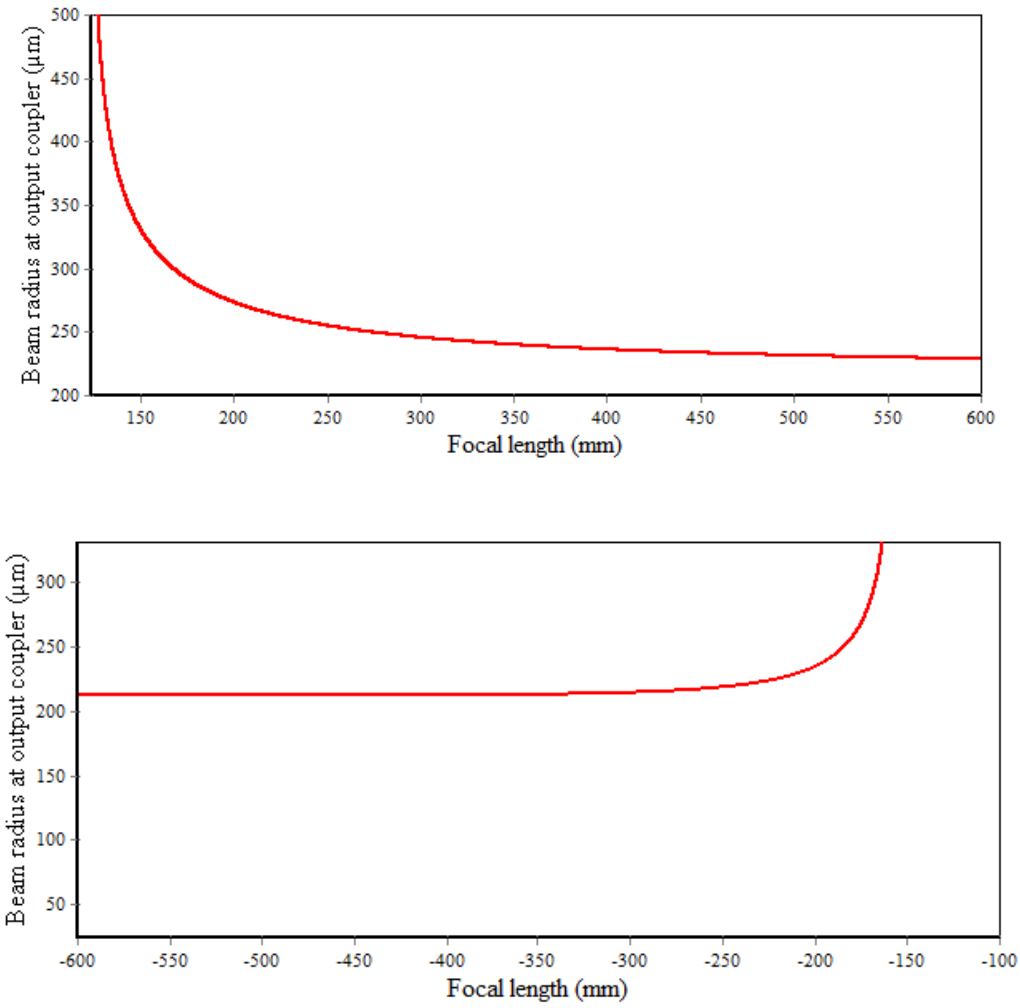

Figure 3.6- Beam radius variation at the output coupler with respect to focal length of the thermal lens.

3.3 CW laser

For CW operation we have designed a 5 mirror cavity shown in figure 3.7. An Ng-cut 20-mm-long Nd:KGW slab sample with dimensions of 1.6x6x20 mm^3 and 3-at.% doping concentration was used (Altechna). The crystal had flat end faces which were antireflection coated at 1067 nm. Cavity mirrors M1-M4 were highly reflecting at 1067 nm. Cavity focusing mirrors M2 and M4 had 400 mm and 500 mm radii of curvature, respectively. M3 was a flat dichroic mirror. A dichroic mirror has different reflection or transmission properties for two different wavelengths. In our experiment, M3 was completely transmitting the pump wavelength and also fully reflecting the

laser wavelength within the cavity. The distances L1, L2, L3 & L4 were 315, 455, 481, and 462 mm, respectively (see also Table 3.1).

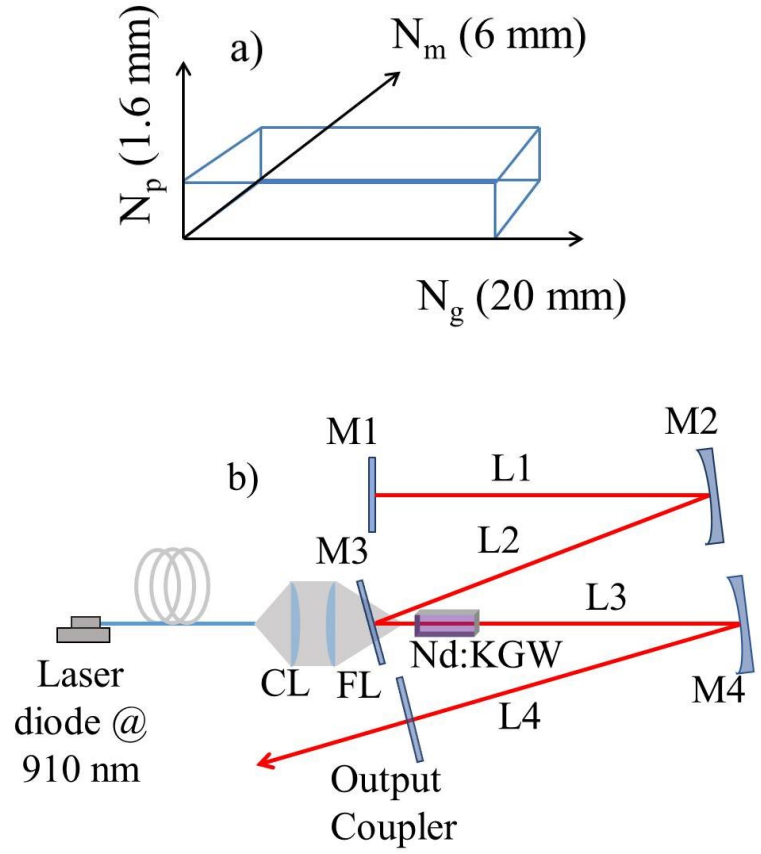

Figure 3.7- a) Nd:KGW crystal dimension, b) Experimental setup for continuous wave operation.

The unpolarized output of the fiber coupled laser diode was focused into the crystal by using a 1:5 imaging system which produced a pump spot diameter of 550 µm inside the crystal. A 1:5 imaging system was built using a collimator lens and a focusing lens with an f = 40 mm and f = 200 mm, respectively. According to the simulation, the cavity beam diameter at the crystal was also about 550 µm which was the same as the beam diameter produced by the imaging system. Indium foil was used to wrap the laser crystal to improve the thermal conduction between the laser crystal and the aluminum heat sink. The laser crystal was water cooled at 16 ˚C as shown in figure 3.8(a). A typical experimental laser setup is also shown in figure 3.8(b). Output power was measured using different output couplers with 5%, 7.5%, 10% and 15% transmission. The best

performance in terms of output power was achieved using an output coupler with 10% transmission.

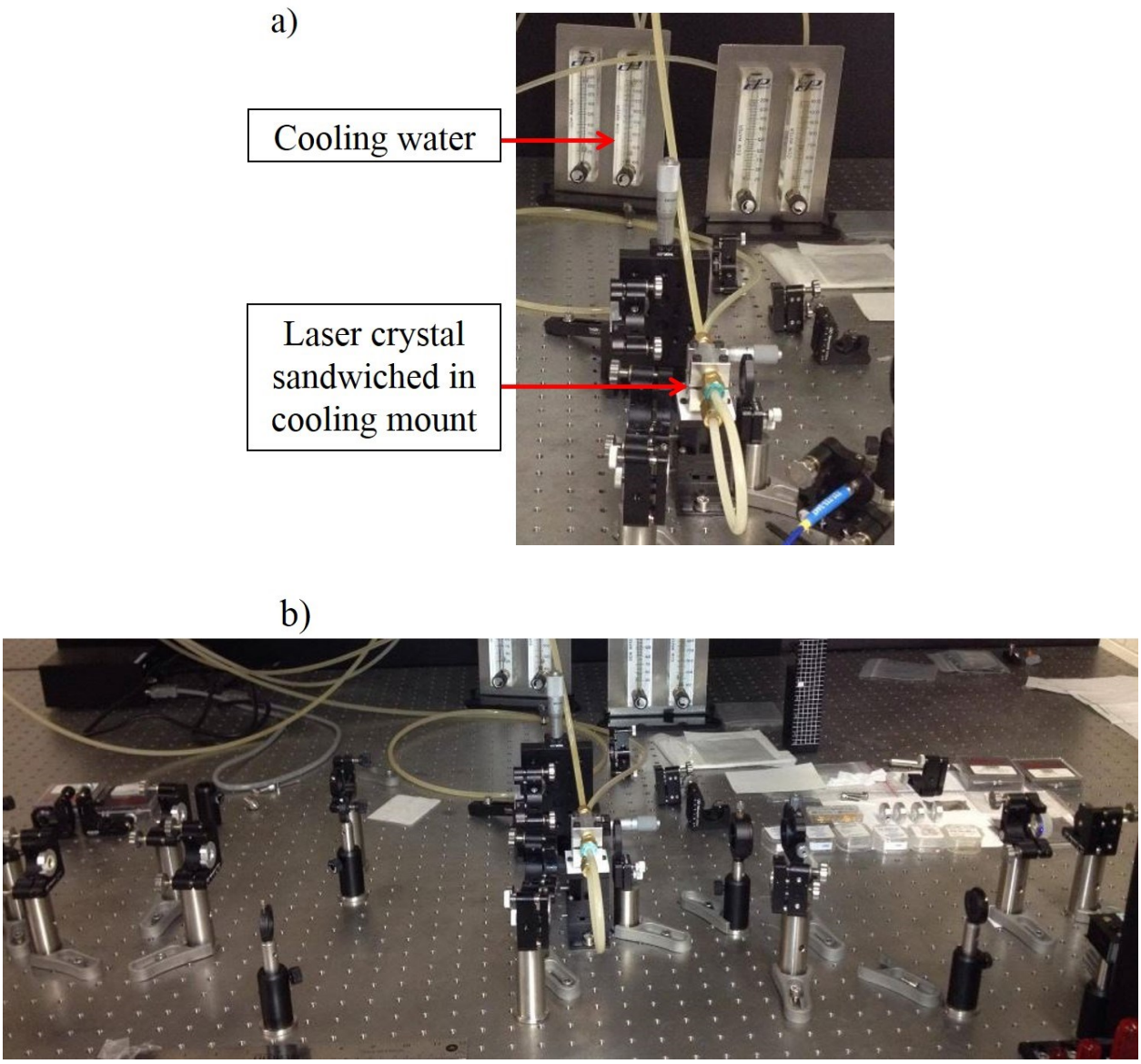

Figure 3.8- a) Water cooling mount of the Nd:KGW laser crystal, b) a typical experimental laser setup.

3.3.1 CW results

At 15 W of pump power about 8.3 W was absorbed by the crystal and 2.9 W of average output power was generated at 1067 nm. The input-output power curve is displayed in figure 3.9(a). With respect to the absorbed pump power, the slope efficiency was found to be 43% and the optical-to-optical efficiency reached was 35%. For the case of ~808 nm pumping, the highest slope efficiency and optical-to-optical efficiency for Nd:KGW crystal were reported as 75% [37] and 66% [36], respectively, with respect to the absorbed pump power. The best slope efficiency for ~880 nm pumping was 66.4% with optical-to-optical efficiency reaching 63.9% [15].

Comparison of continuous wave results is shown in table 3.2 [15, 36]. It is clear from the table that 808 nm and 880 nm pumping have higher output power than our experimental result. Both the slope and optical–to-optical efficiency were lower in our case as compared to other results. The total efficiency was calculated by considering the electrical-to-optical efficiency of the pump diode which is 50% in our case. We got 2.9 W of optical power from the laser when the electrical power at the input of the pump diode was 32 W which corresponds to a total efficiency of 9.1%. The total efficiency was not mentioned in other two experimental works.

Table 3.2- Comparison of CW results

Author	Pump λ (nm)	CW output power (W)	Slope efficiency (%)	Optical-to-optical efficiency (%)	Total efficiency (%)	Cavity mirrors
E. Rafailov et al.	808	3.3	74	66	-	2
A.A. Bui et al.	880	9.4	66.4	63.9	-	2
This work	910	2.9	43	35	9.1	5

We believe that in our proof-of-principle experiment the lower values of slope and optical efficiency can be explained by the higher intracavity losses introduced by a larger number of mirrors (five-mirror cavity was used in contrast to two-mirror cavities used in previous works), probably not completely optimal transmission of the used output coupler, as well as fairly high reflectivity of the crystal AR coatings at the laser wavelength which was specified as 0.25% (per surface). Not only that, this lower slope efficiency can also come from lower power extraction efficiency and lower geometrical coupling due to lower saturation parameter [39]. Saturation parameter is defined as following,

$$S = \frac{2P}{I_s \pi w_l^2} \tag{3.1}$$

Here, P= intracavity circulating power,

I_s= saturation intensity and

w_l = laser beam radius.

The spectrum of the generated laser radiation is shown in figure 3.9(b). Its linewidth at half maximum was measured to be 0.13 nm, limited by the resolution of our spectrometer (0.1 nm). The output laser radiation was linearly polarized along the N_m-axis.

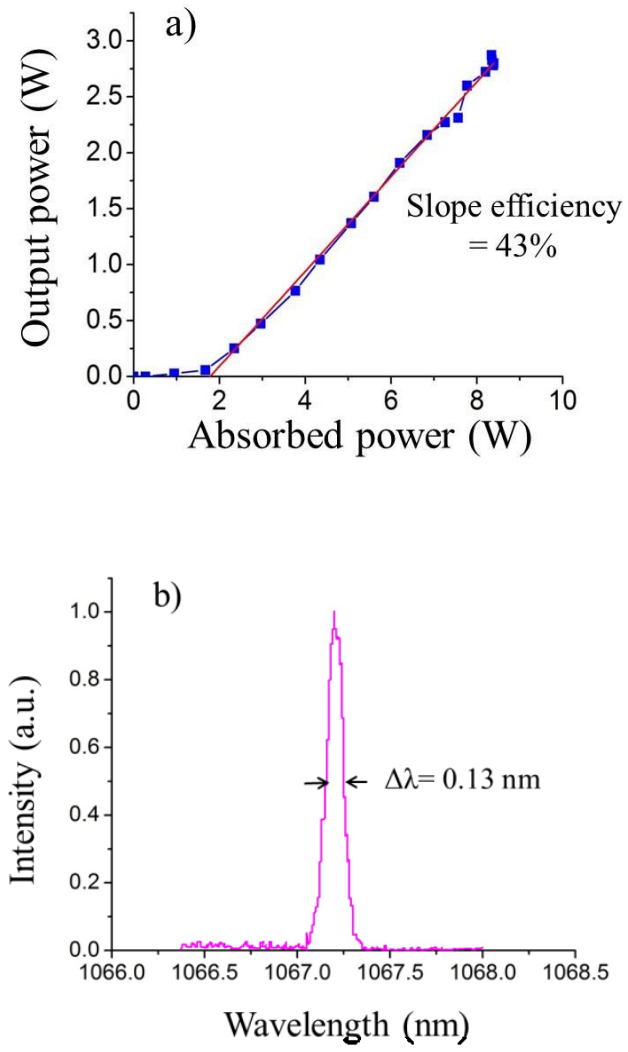

Figure 3.9- a) Measured output power with linear fit, b) CW laser spectrum.

For 6 – 15 W of incident pump power, the pump absorption varied linearly from 71% to 55% of the input power as shown in figure 3.10. The variation of absorbed power can be explained by the change in wavelength of the pump diode with drive current (see figure 3.2(a)). Pump absorption efficiency in our case can be enhanced by using a longer crystal with higher doping concentration or by using a wavelength-stabilized pump diode.

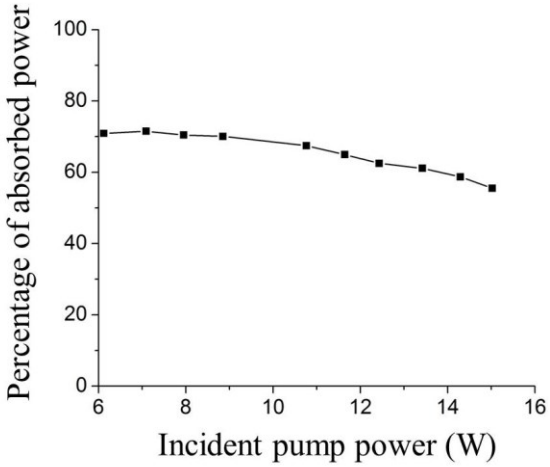

Figure 3.10- Percentage of absorbed pump power vs. incident pump power.

The laser had a very good beam quality. The beam quality factor (M^2) represents the degree by which a laser beam is above the diffraction limit of an ideal Gaussian beam. It is defined as

$$M^2 = \frac{\pi\theta w_0}{\lambda} \tag{3.2}$$

where, θ = half angle beam divergence, w_0= beam radius, and λ = wavelength of the laser beam. For an ideal Gaussian beam M^2 value is 1 [22].

The M^2 value can be measured by placing a focusing lens at a fixed distance from the output coupler and then by measuring the spot sizes of the focused beam along the propagation direction using a CCD beam profiler. The focal length of the focusing lens was 150 mm. The schematic of this measurement is shown in figure 3.11. The M^2 value and the beam waist w_0 of the laser beam were calculated by fitting the measured spot sizes to the Gaussian beam propagation equation which is given below.

$$W(z) = W_0\sqrt{1 + \left(\frac{M^2 z\lambda_0}{n\pi {w_0}^2}\right)^2} \tag{3.3}$$

Here, λ_0 is the laser wavelength and z is the position of the beam along the propagation axis.

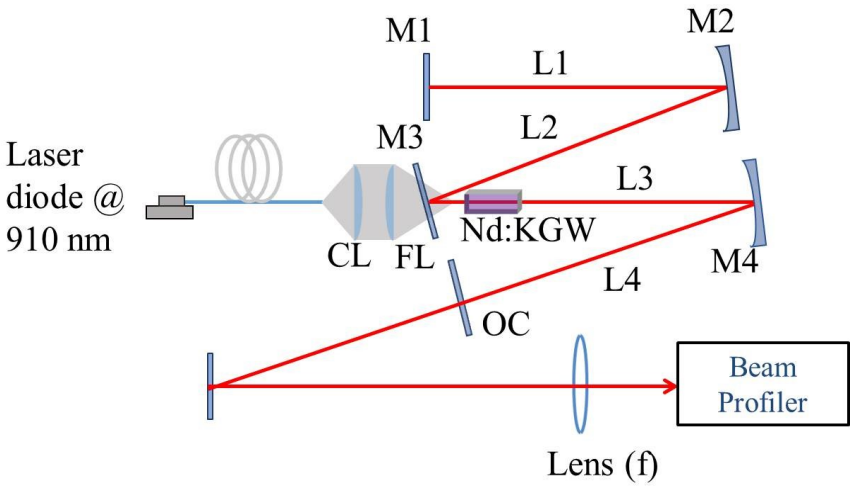

Figure 3.11- Measurement of beam radius variation.

The beam quality factor M^2 was found to be 1.16 in the horizontal direction and 1.36 in the vertical direction which is close to a perfect Gaussian beam. The measurement data along with the output beam shape are presented in Figure 3.12.

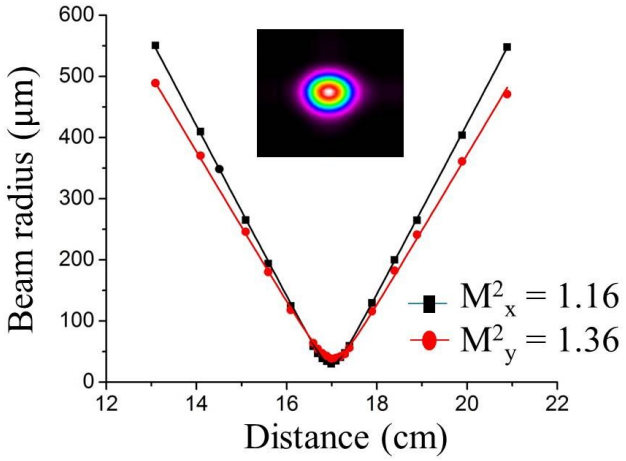

Figure 3.12- Laser beam quality at 2.9 W of output power. Inset: transverse intensity profile of the laser beam.

3.4 Thermal lensing measurement

The purpose of this measurement was to find the focal length of the induced thermal lens in the Nd:KGW crystal. The thermal lens was modeled as a thin lens inside the laser crystal. The focal length of this imaginary lens varied with different absorbed pump power. Therefore, the strength of the thermal lens focusing power was measured for different absorbed pump power levels. First, the M^2 values were measured in horizontal and vertical directions for different absorbed powers (see section 3.3.1). Then, a variable lens inside the crystal within a laser cavity can be simulated using the ABCD matrix analysis while the experimental M^2 value was taken into account. The focal length of the thermal lens was determined as a value at which the beam waist after the focusing lens from the experiment and the one from the ABCD model matched. The same simulation was repeated for different absorbed powers to find the respective focal lengths. The ABCD matrix analysis with variable thermal lens and beam propagation outside of the cavity was studied with commercial LASCAD [40] software.

3.4.1 Thermal lensing results

The measured beam waist data and non-linear fitting curves for output powers of 1.6 W and 2.7 W are shown in figure 3.13. M_x^2 and M_y^2 represent the beam quality in horizontal plane and vertical plane, respectively.

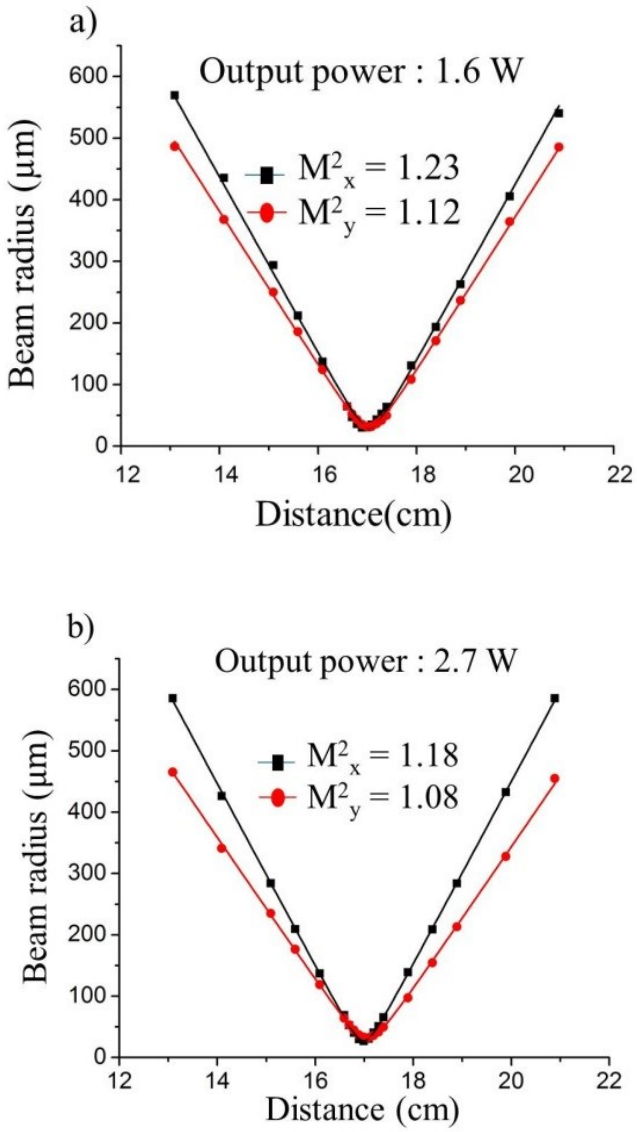

Figure 3.13- Laser output beam quality M^2 at output power of 1.6 W and 2.7 W.

The output power and laser beam quality factor values with respect to the absorbed pump power are shown in figure 3.14. The M^2 value was <1.4 throughout the experiment. The measured M^2 values and beam waist values were used in LASCAD software to simulate the focusing power of the induced thermal lens.

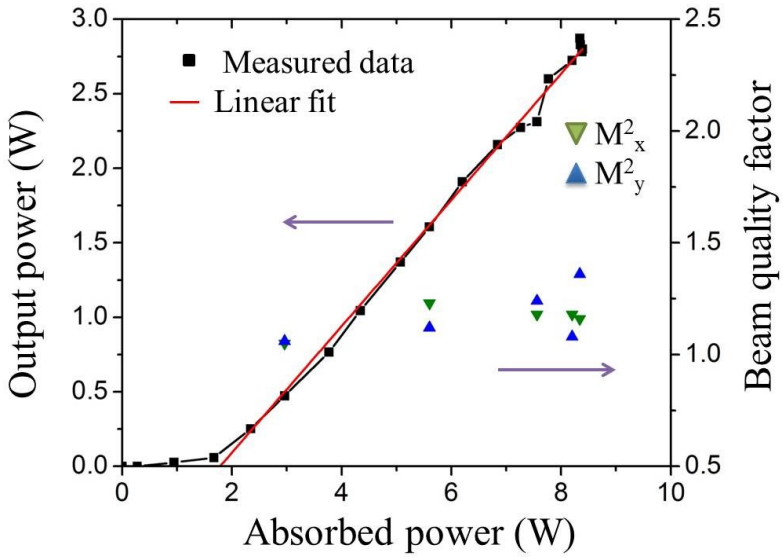

Figure 3.14- Output power and beam quality factor values vs. absorbed pump power.

The thermal lens focusing power in both horizontal and vertical direction is shown in figure 3.15. It is obvious that the thermal lens focusing power is almost same in both directions.

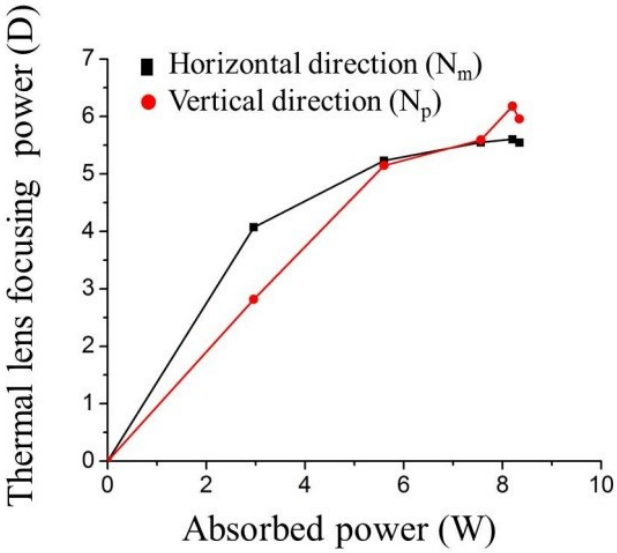

Figure 3.15- Thermal lens focusing power with respect to absorbed pump power.

It is also instructive to compare the observed thermal lensing effect as shown in table 3.3 with all different reported pump wavelengths (i.e. 808 nm, 880 nm and 910 nm) used to pump the Nd:KGW crystal .The thermal lens focusing power with 808 nm and 880 nm pumping was reported in [13]. At 808 nm pumping, it was measured to be ~9 diopters in the horizontal direction and ~10 diopters in the vertical direction with absorbed pump power of 2.35 W. The focusing power of thermal lens for 880 nm pumping was also measured to have the same values in both directions at a higher absorbed pump power of 4.44 W. This result can be explained by the higher quantum defect for pumping with 808 nm wavelength as compared to pumping with 880 nm. In our experiment, the thermal lens dioptric power was measured using a modified ABCD-matrix analysis which took into account laser beam quality [41]. At 8.3 W of absorbed pump power it was found to be ~5.5 diopter in the horizontal direction and ~6.0 diopter in the vertical direction. These measurements clearly indicate that even at the much higher absorbed pump power level the thermal lensing effect is significantly lower for 910 nm pumping as compared to both 880 nm and 808 nm pumping. Therefore, the proposed new pump wavelength at 910 nm holds strong potential for power scaling of Nd:KGW lasers owing to the strongly reduced thermal effects.

Table 3.3- Comparison of thermal lens focusing power

Author	Pump wavelength (nm)	Absorbed power (W)	Thermal lens power, horizontal direction (D)	Thermal lens power, vertical direction (D)
Huang Ke et al.	808	2.35	9	10
Huang Ke et al.	880	4.44	9	10
This work	910	8.3	5.5	6

Absorbed power is not the only parameter on which the thermal lens focusing power depends on. It also depends on the pump beam radius, crystal geometry, pump absorption efficiency, etc.

The thermal lens dioptric power can be defined as following [42]:

$$D_{th} = \frac{1}{f_{th}} = \frac{\eta_a P_{abs} \chi}{2\pi K w_p{}^2} \tag{3.4}$$

Here, f_{th} = focal length of thermal lens,

K = thermal conductivity of crystal,

P_{abs} = absorbed pump power,

η_a = pump absorption efficiency,

χ = polarization-averaged thermo-optic coefficient,

$w_p{}^2$ = pump beam radius,

Although a lower thermal lensing in the case of 910 nm pumping is obvious, it is worth noting, however, that a direct comparison with the quoted values above in table 3.3 is not straightforward because of the different experimental conditions such as the pump spot size, crystal geometry, pump absorption length, cooling geometry, and coolant temperature. For example, we used the pump beam radius of 275 μm while Huang Ke et al. used a pump beam radius of 130 μm. According to the equation 3.4, the thermal lens focusing power is inversely proportional to the square of the pump beam radius. Therefore, the lower pump beam radius contributed to the higher focusing power in Huang Ke et al. work. Nonetheless, in the case of ~808 nm pumping a stronger thermal lensing by a factor of two should be observed in comparison with 910 nm pump wavelength under the same experimental conditions [18].

Chapter 4: Conclusion and future work

Multi-Watt CW operation of a Nd:KGW at 1067 nm with hot band diode pumping was successfully demonstrated. To the best of our knowledge, this is the first time that this approach was used with Nd:KGW laser crystal. The pump wavelength of ~910 nm significantly (>46%) reduced the quantum defect and thus the amount of heat deposited in the crystal. Moreover, the laser cavity was designed to have a very good overlap between the pump and cavity mode for higher efficiency. The laser produced 2.9 W of average output power with 8.3 W of absorbed pump power. The laser beam quality throughout the experiment was very good ($M^2 < 1.4$) in both horizontal and vertical directions. The slope efficiency and optical-to-optical efficiency were found to be 43% and 35%, respectively. We also measured the thermal lensing focusing power for different absorbed pump power levels. The focal lengths of the induced thermal lenses were obtained from the laser output beam waist measurements at various output powers using a modified ABCD matrix analysis. It is important to mention that M^2 values were taken into account for those focal length simulations. The thermal lens dioptric power at 8.3 W of absorbed pump power was found to be ~5.5 diopter in the horizontal direction and ~6.0 diopter in the vertical direction.

Reduced thermal effects as a result of hot band diode pumping opens a way to further power scaling of Nd:KGW lasers by using high power laser diodes that are currently widely used for pumping of Yb-doped fiber lasers. Therefore, further power scaling with hot band diode pumping by a 40 W laser diode would be a future work for Nd:KGW crystal. Frequency doubling of such a laser can provide green radiation suitable for excitation of, for example, Ti:sapphire [43] or Alexandrite lasers [44]. Not only that, continuous wave operation of Nd:KGW at 1350 nm with hot band diode pumping could also be studied in the future. Another interesting topic would be the development of a pulsed Nd:KGW laser based on mode locking technique to generate picosecond optical pulses. Such sources of pulsed laser radiation are widely used in various experiments such as nonlinear frequency conversion [45, 46, 47, 48, 49], nonlinear microscopy [50], nonlinear [51], and time-resolved [52] spectroscopy.

References

1. A.A. Demidovich, A.P. Shkadarevich, M.B. Danailov, P.Apai, T. Gasmi, V.P. Gribkovskii, A.N. Kuzmin, G.I. Ryabtsev, L.E. Batay, "Comparison of cw laser performance of Nd:KGW, Nd:YAG, Nd:BEL, and Nd:YVO_4 under laser diode pumping," Applied Physics B 67, 11-15 (1998).
2. T. Graf, J.E. Balmer, "Lasing properties of diode-laser-pumped Nd:KGW," Optical Engineering 34, 2349-2352 (1995).
3. Y. Kalisky, L. Kravchik, C. Labbe, "Repetitive modulation and passively Q-switching of diode-pumped Nd:KGW laser," Optics Communications 189, 113-125 (2001).
4. A. Major, N. Langford, T. Graf, D. Burns, A. I. Ferguson, "Diode-pumped passively mode-locked Nd:$KGd(WO_4)_2$ laser with 1W average output power," Optics Letters 27, 1478-1480 (2002).
5. A. Major, N. Langford, T. Graf and A. I. Ferguson, "Additive-pulse mode locking of a diode-pumped Nd: laser," Applied Physics B 75, 467-469 (2002).
6. A.S. Grabtchikov, A.N. Kuzmin, V.A. Lisinetskii, V.A. Orlovich, G.I. Ryabtsev, A.A. Demidovich, "All solid-state diode-pumped Raman laser with self-frequency conversion," Applied Physics Letters 75, 3742-3744 (1999).
7. A. Major, J.S. Aitchison, P.W.E. Smith, N. Langford, A.I. Ferguson, "Efficient Raman shifting of high-energy picosecond pulses into the eye-safe 1.5 μm spectral region using a $KGd(WO_4)_2$ crystal", Optics Letters 30, 421-423 (2005).
8. A. Major, D. Sandkuijl, V. Barzda, "Efficient frequency doubling of a femtosecond Yb:KGW laser in a BiB3O6 crystal," Optics Express 17, 12039-12042 (2009).
9. A. Major, J.S. Aitchison, P.W.E. Smith, F. Druon, P. Georges, B. Viana, G.P. Aka "Z-scan measurements of the nonlinear refractive indices of novel Yb-doped laser crystal hosts," Applied Physics B 80, 199-201 (2005).
10. A. Major, I. Nikolakakos, J.S. Aitchison, A.I. Ferguson, N. Langford and P.W.E. Smith, "Characterization of the nonlinear refractive index of the laser crystal Yb: $KGd(WO_4)_2$," Applied Physics B: Lasers and Optics 77, 433-436 (2003).
11. A.A. Demidovich, A.S. Grabtchikov, V.A. Lisinetskii, V.N. Burakevich, V.A. Orlovich, W. Kiefer, "Continuous-wave Raman generation in a diode-pumped Nd^{3+}: $KGd(WO_4)_2$ laser," Optics Letters 30, 1701-1703 (2005).
12. P.A. Loiko, K.V. Yumashev, N.V. Kuleshov, A.A. Pavlyuk., "Thermo-optic coefficients and thermal lensing in Nd-doped Nd: $KGd(WO_4)_2$ laser crystals," Applied Optics 49, 6651-6659 (2010).

13. K. Huang, W.Q. Ge, T. Z. Zhao, C. Y. Feng, J. Yu, J. G. He, H. Xiao, Z, W, Fan, "High-power passively Q-switched Nd:KGW laser pumped at 877 nm," Applied Physics B 122, 171 (2016).
14. Andrew J. Lee, H. M. Pask, D. J. Spence and J.A. Piper, "Generation of yellow, continuous-wave emission from an intracavity, frequency-doubled Nd:KGW self-Raman laser," OSA, Advanced Solid-State Photonics (2010).
15. A. A. Bui, U.I. Dashkevich, V.A. Orlovich, and I.A. Khodasevich, "Diode-pumped Nd: $KGd(WO_4)_2$ laser: lasing at fundamental and second harmonic frequencies," Journal of Applied Spectroscopy 82, 4 (2015).
16. D. Sangla, M. Castaing, F. Balembois, and P. Georges, "Highly efficient Nd:YVO_4 laser by direct in-band diode pumping at 914 nm," Optics Letters 34, 2159-2161 (2009).
17. T. Waritanant and A. Major, "High efficiency passively mode-locked Nd:YVO_4 laser with direct in-band pumping at 914 nm," Optics Express 24, 12851-12855 (2016).
18. T. Waritanant and A. Major, "Thermal lensing in Nd:YVO_4 laser with in-band pumping at 914 nm," Applied Physics B 122, 135 (2016).
19. R. C. Talukder, Md Z. E. Halim, T. Waritanant, A. Major, "Continuous Wave Nd: KGW Laser With Hot Band Diode Pumping," Photonics North-2016.
20. R. C. Talukder, Md Z. E. Halim, T. Waritanant, A. Major, "Multi-Watt Continuous Wave Nd: KGW Laser With Hot Band Diode Pumping," CLEO: Science and Innovations, 2016.
21. R. C. Talukder, Md Z. E. Halim, T. Waritanant, A. Major, "Multiwatt continuous wave Nd: KGW laser with hot-band diode pumping," Optics Letters 41, 3810-3812 (2016).
22. W. Koechner, Solid-State Laser Engineering, Springer, 2005.
23. H. Hiller, "Crystallography and Cohomology of Groups," The American Mathematical Monthly 93, 765-779 (1986).
24. I. V. Mochalov, "Laser and nonlinear properties of the potassium gadolinium tungstate laser crystal $KGd(WO_4)_2:Nd^{3+}$-(KGW:Nd)," Optical Engineering 36, 1660-1669, (1997).
25. Y. Chen, Y. Lin, X. Gong, Q. Tan, J. Zhuang, Z. Luo, Y. Huang, "Polarized spectroscopic properties of Nd^{3+}-doped $KGd(WO_4)_2$ single crystal," Journal of Luminescence 126, 653-660 (2007).
26. A. Major, L. Giniūnas, N. Langford, A.I. Ferguson, D. Burns, E. Bente, and R. Danielius, "Saturable Bragg reflector-based continuous-wave mode locking of Yb:$KGd(WO_4)_2$ laser," Journal of Modern Optics 49, 787-793 (2002).
27. H. Zhao and A. Major, "Powerful 67 fs Kerr-lens mode-locked prismless Yb:KGW oscillator," Optics Express 21, 31846-31851 (2013).

28. H. Zhao and A. Major, “Megawatt peak power level sub-100 fs Yb:KGW oscillators,” Optics Express 22, 30425-30431 (2014).
29. R. Akbari, H. Zhao, K.A. Fedorova, E.U. Rafailov, A. Major, “Quantum-dot saturable absorber and Kerr-lens mode-locked Yb:KGW laser with >450 kW of peak power,” Optics Letters 41, 3771-3774 (2016).
30. R. Moncorge, B. Chambon, J.Y. Rivore, N. Garnier, E. Descroix, P. Laporte, H. Guillet, S. Roy, J. Mareschal, D. Pelenc, J. Doury and P. Farge, “Nd-doped crystals for medical laser applications,” Optical Materials 8, 109-119 (1997).
31. J. M. Esmeria Jr., H. Ishii, M. Sato, and H. Ito, “Efficient continuous-wave lasing operation of Nd: $KGd(WO_4)_2$ at 1.067 mm with diode and Ti:sapphire laser pumping,” Optics Letters, 20, 1538-1540 (1995).
32. A. Major, D. Sandkuijl, V. Barzda, “A diode-pumped continuous-wave Yb:KGW laser with Ng-axis polarized output”, Laser Physics Letters 6, 779-781 (2009).
33. ALPHALAS GMBH, Germany.
34. C. J. Flood, D. R. Walker, H. M. van Driel, “CW diode pumping and FM mode locking of a Nd:KGW laser,” Applied Physics B 60, 309-312 (1995).
35. H. Ke, GE Wen-Qi, Z. Tian-Zhuo, HE Jian-Guo, F. Cheng-Young, F. Zhong-Wei, “Comparative study of Nd:KGW lasers pumped at 808 nm and 877 nm,” Proceedings of SPIE 9671, 96711W-1 (2015).
36. A. Abdolvand, K. G. Wilcox, T. K. Kalkandjiev, and E. U. Rafailov, "Conical refraction Nd: $KGd(WO_4)_2$ laser," Optics Express 18, 2753-2759 (2010).
37. G. Boulon, G. Metrat, N. Muhlstein, A. Brenier, M.R. Kokta, L. Kravchik, Y Kalisky, “Efficient diode-pumped Nd: $KGd(WO_4)_2$ laser grown by top nucleated floating crystal method,” Optical Materials 24, 377-383 (2003).
38. reZonator software.
39. F. Krausz, E. Wintner, A. J. Schmidt, and A. Dienes, “Continuous Wave Thin Plate Nd : Glass Laser,” IEEE Journal of Quantum Electronics 26, 158-168 (1990).
40. LASCAD GmbH, Munich.
41. H. Mirzaeian, S. Manjooran and A. Major, “A simple technique for accurate characterization of thermal lens in solid state lasers,” Proceedings of SPIE 9288, 928802 (2014).
42. S. Chenais, F. Druon, S. Forget, F. Balembois, P. Georges, “Review On thermal effects in solid-state lasers: The case of ytterbium-doped materials,” Progress in Quantum Electronics 30, 889-153 (2006).

43. K. Lamb, D. E. Spence, J. Hong, C. Yelland, and W. Sibbett, "All-solid-state self-mode-locked Ti:sapphire laser," Optics Letters 19, 1864-1866 (1994).
44. S. Ghanbari, R. Akbari, A. Major, "Femtosecond Kerr-lens mode-locked Alexandrite laser," Optics Express 24, 14836-14840 (2016).
45. R. Akbari and A. Major, "Optical, spectral and phase-matching properties of BIBO, BBO and LBO crystals for optical parametric oscillation in the visible and near-infrared wavelength ranges," Laser Physics 23, 035401 (2013).
46. H. Zhao, I. T. Lima Jr., and A. Major, "Near-infrared properties of periodically poled $KTiOPO_4$ and stoichiometric MgO-doped $LiTaO_3$ crystals for high power optical parametric oscillation with femtosecond pulses," Laser Physics 20, 1404-1409 (2010).
47. I. T. Lima Jr., V. Kultavewuti, and A. Major, "Phasematching properties of congruent MgO-doped and undoped periodically poled $LiNbO_3$ for optical parametric oscillation with ultrafast excitation at 1 μm," Laser Physics 20, 270-275 (2010).
48. A. Major, K. Sukhoy, H. Zhao, and I. T. Lima Jr., "Green sub-nanosecond microchip laser based on BiBO crystals," Laser Physics 21, 57-60 (2011).
49. H. Zhao, K. Sukhoy, I. T. Lima Jr., and A. Major, "Generation of green second harmonic with 60% conversion efficiency from a Q-switched microchip laser in MgO:PPLN crystal," Laser Physics Letters 9, 355-358 (2012).
50. D. Sandkuijl, R. Cisek, A. Major, and V. Barzda, "Differential microscopy for fluorescence-detected nonlinear absorption anisotropy based on a staggered two-beam femtosecond Yb:KGW oscillator," Biomedical Optics Express 1, 895-901 (2010).
51. A. Major, F. Yoshino, J.S. Aitchison, P.W.E. Smith, E. Sorokin and I.T. Sorokina, "Ultrafast nonresonant third-order optical nonlinearities in ZnSe for all-optical switching at telecom wavelengths," Applied Physics Letters 85, 4606-4608 (2004).
52. I.P. Nikolakakos, A. Major, J.S. Aitchison and P.W.E. Smith, "Broadband characterization of the nonlinear optical properties of common reference materials," IEEE Journal of Selected Topics in Quantum Electronics 10, 1164-1170 (2004).